Available online at www.sciencedirect.com
SCIENCE DIRECT®
Acta Materialia 52 (2004) 35–47
Acta MATERIALIA
www.actamat-journals.com

Phase transformation and magnetic anisotropy of an iron–palladium ferromagnetic shape-memory alloy

J. Cui [a,*], T.W. Shield [b], R.D. James [b]

[a] Department of Materials and Nuclear Engineering, University of Maryland, College Park, MD 20742, USA
[b] Department of Aerospace Engineering and Mechanics, University of Minnesota, Minneapolis, MN 55455, USA

Received 25 March 2003; received in revised form 22 July 2003; accepted 23 July 2003

Abstract

Martensitic phase transformations in an Fe_7Pd_3 alloy were studied using various experimental techniques: visual observation, differential scanning calorimeter (DSC) measurements and X-ray diffraction. Magnetic measurements on this alloy were made using a vibrating sample magnetometer (VSM) and a Susceptibility Kappa bridge. The VSM measurements were made with the sample in a compression fixture to bias the martensite phase to a single variant. Both X-ray and DSC measurements show that the FCC–FCT transformation is a weak first-order thermoelastic transition. The average lattice parameters are $a = 3.822 \pm 0.001$ Å and $c = 3.630 \pm 0.001$ Å for the FCT martensite, and $a_0 = 3.756 \pm 0.001$ Å for the FCC austenite. The latent heat of the FCC–FCT transformation is 10.79 ± 0.01 J/cm^3. A Susceptibility Kappa bridge measurement determined the Curie temperature to be 450 °C. The saturation magnetization from VSM data is $m_s = 1220 \pm 10$ emu/cm^3 at −20 °C for the martensite and $m_s = 1080 \pm 10$ emu/cm^3 at 60 °C for the austenite. The easy axes of a single variant of FCT martensite are the [1 0 0] and [0 1 0] directions (the a-axes of the FCT lattice) and the [0 0 1] direction (FCT c-axis) is the hard direction. The cubic magnetic anisotropy constant K_1 is $-5 \pm 2 \times 10^3$ erg/cm^3 for the austenite at 60 °C, and the tetragonal anisotropy constant $K_1 + K_2$ is $3.41 \pm 0.02 \times 10^5$ erg/cm^3 for the martensite at a temperature of −20 °C and under 8 MPa of compressive stress in the [0 0 1] direction.

Keywords: Ferromagnetic; Magnetic anisotropy; Martensitic phase transformation; Shape-memory alloys; X-ray diffraction

1. Introduction

Shape-memory effects are due to a diffusionless structural phase transformation from a high-temperature high-symmetry (austenite) phase to a low-temperature low-symmetry (martensite) phase. The lower symmetry of the martensite results in the formation of multiple variants each with its own associated shape change. If the martensitic transformation is induced by temperature in the absence of biasing fields, all of the variants are equally likely to form because they all have the same free energy. When a bias field is applied to this mixture of variants, certain variants will be favored and appear in larger amounts than the other variants. This can be quantified through minimization of the free energy of the system. The material under consideration here transforms from a cubic austenite phase to a tetragonal martensitic phase as shown in Fig. 1. An applied compressive stress along the e_1 direction will favor the variant E_1 over the other variants that are longer in their e_1 dimension, this procedure is discussed in detail in [1].

For materials that undergo a shape-memory transformation and are ferromagnetic the variant structure may also be biased by a magnetic field. When a magnetic field is applied to a ferromagnetic material that undergoes a reversible martensitic transformation, there exist three possible mechanisms that can produce a shape change. First, applying a magnetic field to the austenite phase can induce a structural transition, as in Fe–Ni alloys [2], although this requires very large fields, about 10 T for a 20 °C shift in transformation temperature. This effect is due, in part, to a large difference in the saturation magnetizations of the two phases [3]. Second,

* Corresponding author. Tel.: +1-301-405-5229; fax: +1-301-405-6327.
E-mail address: cuijun@aem.umn.edu (J. Cui).

1359-6454/$30.00 © 2003 Acta Materialia Inc. Published by Elsevier Ltd. All rights reserved.
doi:10.1016/j.actamat.2003.08.024

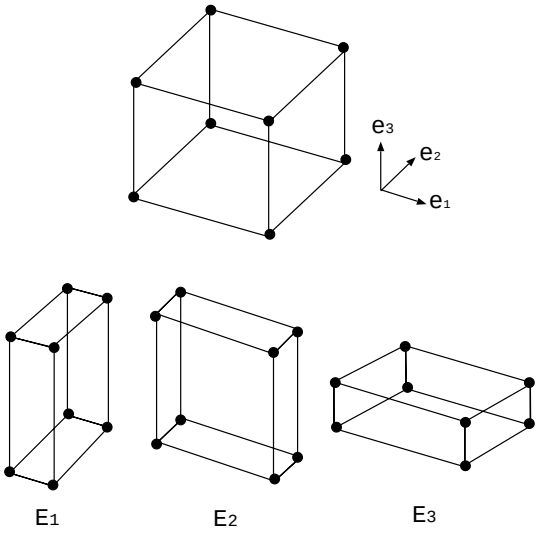

Fig. 1. Lattice deformations corresponding to the three variants of martensite are sketched. The strains are exaggerated for clarity. The short axis of the tetragonal martensite is the *c*-axis.

a magnetic field can rotate the spontaneous magnetization with respect to the crystal lattice, as is the case in Terfenol-D [4]. This is conventional (giant in the case of Terfenol) magnetostriction, which does not require a phase transformation. In this case the material has very small magnetic anisotropy, so that there is little or no energy cost for rotating the magnetization. Third, a magnetic field can rearrange martensite variants giving rise to the ferromagnetic shape-memory (FSM) effect, as in the Ni_2MnGa [5] and Fe_7Pd_3 [7] alloys considered here. This rearrangement of variants can result in the large strains typical of shape-memory materials. However, it requires high mobility of the twin interfaces between variants and large magnetic anisotropy to constrain the spontaneous magnetization along the variant easy axis. This constraint is necessary to develop the large driving forces on the twin interfaces needed for variant rearrangement.

This paper is concerned with the FSM effect and in particular the role magnetic anisotropy plays in it. Fig. 2 illustrates the FSM mechanism for materials with low and high magnetic anisotropy. For an FSM material with high magnetic anisotropy it takes less energy (under suitable loading conditions) to move the twin boundaries and change the variant volume fractions than to rotate the magnetization. Thus for a horizontally applied field, as shown in Fig. 2, the variant with a horizontal magnetization grows at the expense of the other variant (through twin boundary motion) in the high anisotropy case while in the low anisotropy case the magnetization rotates resulting in a much smaller change in shape.

To date, Ni_2MnGa and Fe_7Pd_3 are the only two alloys reported exhibiting the FSM effect at ordinary fields. The alloy Ni_2MnGa has been studied extensively

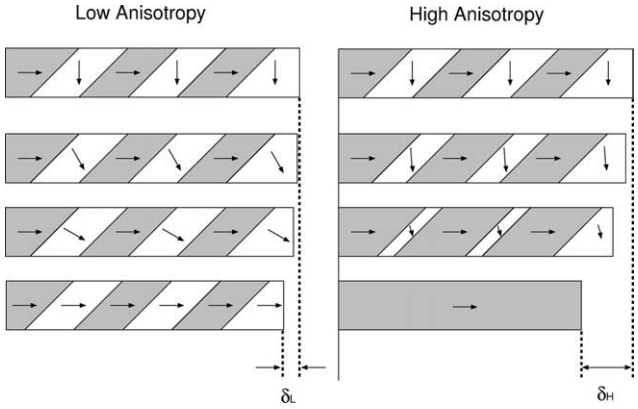

Fig. 2. Schematic drawing of the mechanisms of magnetostriction (left) and FSME (right) is shown. The arrows represent the spontaneous magnetization direction. The four drawings shown the situation as the applied horizontal magnetic field is increases from zero (top sketches) to saturation (bottom sketches).

(see [5,6], and [8–12] for example) while less attention has been paid to Fe_7Pd_3. Although the reported field induced strain in Fe_7Pd_3 of 0.6% [7] is considerably less than that in Ni_2MnGa (5.8% in tetragonal and 9.4% in orthorhombic) [6], the Fe_7Pd_3 alloy does possess advantages over Ni_2MnGa. For example, Ni_2MnGa is a brittle material and changes in temperature through the martensitic transformation temperature often lead to fracture. On the other hand, Fe_7Pd_3 is a ductile material, it can be deformed extensively without fracture. Fig. 3(a) shows the picture of a Fe_7Pd_3 polycrystal sample before extensive deformation by peening, and Fig. 3(b) shows that the thickness of the sample was reduced by about five times by this deformation. The magnetic properties of these two alloys are different in many aspects as well. For example, the magnetic easy axis is [0 0 1] (*c*-axis of FCT lattice) in Ni_2MnGa [12], and [1 0 0] or [0 1 0] (*a*-axes of FCT lattice) in Fe_7Pd_3 [7]. Thus, a long thin bar of Fe_7Pd_3 in compression meets both the large displacement and low demagnetization factor actuator design criteria simultaneously, while in Ni_2MnGa they compete. This allows an actuator using Fe_7Pd_3 to have a simple solenoid design, which is not possible for Ni_2MnGa used in compression.

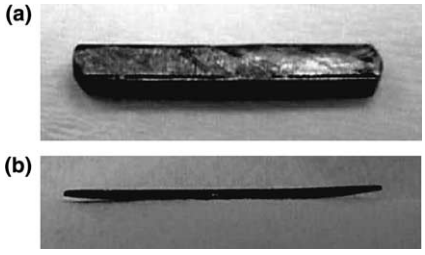

Fig. 3. A polycrystal Fe_7Pd_3 sample before (a) and after (b) it was deformed by hammering is shown.

Thus Fe_7Pd_3 is a promising ferromagnetic shape-memory material, however, the characterization of this alloy is incomplete. Some of these properties have already been extensively studied, especially the martensitic phase transformation in Fe_7Pd_3. Since 1982, Oshima and coworkers [13–28] systematically studied the martensitic phase transformations of the Fe–Pd alloy system. They found that alloys with about 30 at.% Pd undergo successive martensitic phase transformations from FCC to FCT to BCT upon cooling. The FCC–FCT transformation is thermoelastic and the microstructures associated with the FCT phase are twin bands. The FCC–FCT transformation is nearly second-order because of the somewhat gradual development of tetragonality with decreasing temperature. The FCC(or FCT)–BCT transformation is irreversible and the characteristic microstructures of the BCT phase resemble spear-heads. In addition to studying the martensitic transformation, they also used transmission electron microscopy to examine the tweed microstructure, which is a precursor phenomenon in the FCC–FCT martensitic transformation. In 1986, Matsui et al. [29] measured the magnetic anisotropy of an $Fe_{69.5}Pd_{30.5}$ single crystal using a torque magnetometer. They found that the easy axis of the FCT martensite is the short c-axis and the anisotropy constant K_1 (for uniaxial symmetry) is about 6×10^5 erg/cm^3 near the FCC–FCT transformation temperature. This result indicates that Fe_7Pd_3 has magnetic properties that are similar to Ni_2MnGa, and disagrees with other workers [7] and the results presented below. They also found that K_1 increases considerably with decreasing temperature and reaches 1.3×10^6 erg/cm^3 at liquid helium temperatures. However, according to the results from Oshima's group [16], at liquid helium temperature the martensite phase should be BCT. Thus the magnetic anisotropy constant of 1.3×10^6 erg/cm^3 may not be for the FCT phase. In addition, Matsui et al. [29] did not apply a bias stress to their sample, which was a thin disk with a 4 mm diameter and 1 mm thickness. Therefore, their reported magnetic anisotropy is an average of all the FCT variants present in their sample. Prediction of FSM behavior requires that the magnetic anisotropy of a single variant be known.

In this study, various measurements were performed to determine the easy axis and to obtain the magnetic anisotropy constants of a single variant of martensite for the Fe_7Pd_3 alloy. In order to make a meaningful magnetic anisotropy measurement in a material that undergoes a structural phase transformation it was first necessary to study the phase transformation using visual observations, differential scanning calorimeter (DSC) measurements and X-ray diffraction. The results of these experiments made it possible to design a series of experiments using a vibrating sample magnetometer (VSM) to measure the magnetic anisotropy of the martensitic phase of this material. The measurements reported below are broken into two sections. First those related to the shape-memory transformation are reported and second the magnetic measurement results are presented.

2. Thermomechanical properties

In this section the properties of the shape-memory transformation are reported. These are the lattice parameters of the cubic austenite and tetragonal martensite and the latent heat of the transformation.

2.1. Sample preparation

A single crystal of Fe_7Pd_3, labeled boule FePd4, was grown using Bridgman method from arc melted buttons made from elemental Fe (99.99%) and Pd (99.98%). Bridgman growth results in segregation of the constituents along the length of the boule. To access this variation in composition a thin slice was taken from the side of the boule. This slice was divided into three samples labeled FePd4S-I, FePd4S-II, and FePd4S-III. The length of theses samples are 13, 13, and 8 mm, respectively. All samples were polished at 80 °C, and the final polishing suspension used was 0.5 μm diamond paste made by Buehler. No heat treatment was done to these samples. Samples used for the composition analysis were also used for visual observation of the phase transformations. Samples used for X-ray analysis are labeled FePd4-T3, FePd4-T5, FePd4-T6 and were heat treated at 900 °C for 120 min followed by rapid quench in NaOH 10 wt.% solution at −8 °C. A sample for latent heat measurement was also cut from boule FePd4 and it is labeled DSC-B2, which weighs 44.6 mg and was not heat treated. A $2 \times 2 \times 6.6$ mm^3 rectangular specimen labeled FePd4-MM6 was cut from the boule and polished for microstructural observation and magneto-mechanical testing (to be reported in a future publication). The susceptibility measurement was performed on a polycrystalline sample labeled FePd-exp222. The compositions of all the specimens are listed in Table 1. This table also lists the heat treatment of the specimens, however, these were not found to have any effect on the material behavior.

2.2. Microstructural observations

Visual observations were performed using a Nikon optical microscope with differential interference contrast (DIC) and a temperature stage. Sample FePd4-MM6 (see Table 1) is selected to illustrate the phase transformation and microstructural development in single crystal Fe_7Pd_3. A series of pictures, shown in Fig. 4, were taken during cooling at 1 °C/min under an applied

Table 1
Summary of Fe_7Pd_3 specimen properties is given

Specimen	Composition (at.% Pd)	Heat treatment
FePd4 S-I, S-II, and S-III	See Fig. 6	None
FePd4-B	29.7 ± 0.1	B
FePd4-T3	29.5 ± 0.1	A
FePd4-T5	29.5 ± 0.1	A
FePd4-T6	29.8 ± 0.1	A
FePd4-MM6	29.5 ± 0.1	None
FePd4-DSC-B2	29.6 ± 0.1	None
FePd-exp222	Nominally 30*	B

Heat treatment A is 120 min at 900 °C followed by a NaOH quench at −8 °C. Heat treatment B is 120 min at 900 °C followed by an ice water quench. The composition of the specimen marked with an * is the nominal (design) composition, but it was not measured.

stress of −1 MPa along the vertical direction in the images. At temperatures above 30 °C, no microstructure was observed and the specimen is in its austenite state. The first microstructure appeared at about 30 °C, it was a cluster of faint bands. As the temperature was lowered, the contrast of these bands became greater and the size of the cluster grew. New bands formed side by side with the existing bands which themselves grew in a direction perpendicular to their length. A second cluster of bands appeared in the sample at about 27 °C and grew in size as the temperature was further lowered. The width of some bands increased at the expense of other bands while some bands kept their width unchanged. When the temperature reached 21 °C, clusters of bands started to merge and most of the area of the sample was covered by twin bands. The evolution of this microstructure appears to indicate that the austenite martensite interfaces (A/M) are mobile. The movement of the twin interfaces (M/M) appears to be mostly due to twin bands merging. Unlike A/M interfaces, M/M interface movement was not perceptible by visual observation, although comparison of pictures taken at different temperatures indicates a change of position of the some interfaces. The cooling process was stopped before −5 °C to avoid the non-reversible FCT–BCT transformation. Microstructural development during the heating process is not exactly a reverse of the cooling process, but it is similar except for approximately 5 °C of hysteresis.

A BCT microstructure was observed in sample FePd4-B (see Table 1), which is shown in Fig. 5. During cooling the microstructures with spear-head shapes started to appear at about −80 °C in a matrix of FCT twin bands. The size and shape of the BCT microstructures that formed remained unchanged even after the sample was heated to 250 °C.

2.3. Composition measurement

Compositions were analyzed at room temperature with JEOL 8900 Electron Probe Microanalyzer (EPMA). Data points were taken every half millimeter along the long axis of the boule using samples FePd4S-I, FePd4S-II, and FePd4S-III. The results of composition analysis are summarized in Fig. 6. The Palladium content changes from 28.7 to 30.7 at.% from the bottom (where solidification occurs first, $x = 0$ in Fig. 6) to the top of the crystal boule. This curve shows that the composition changes slowly in the regions first to solidify and faster toward the end of the boule that solidified last. The fact that the top part of the crystal boule is palladium rich is expected because of the segregation of the impurities to the last part of the solid formed during the crystal growth. Although the composition variation limited the volume of useful material, it provided an opportunity to study the material properties as a function of composition.

2.4. FCC–FCT–BCT phase diagram

Following the composition analysis, samples FePd4S-I, FePd4S-II, and FePd4S-III. were slowly cooled and observed visually to determine the temperature and type of transformation. A translation stage was used to measure the location of the transformation as a function of temperature. During the experiments, the appearance of twin bands and spear-head microstructures were treated as the evidence of the FCT or BCT phases, respectively. Fig. 6 was used to convert location to composition. This combined with the temperature at which the microstructure was observed allows the phase diagram shown in Fig. 7 to be constructed. This phase diagram shows that when the palladium concentration is less than 29.25 at.%, the initial phase transformation is from FCC to BCT. The FCC–BCT transformation temperature increases as the concentration of palladium decreases. When palladium concentration is more than 29.25 at.%, the initial phase transformation is FCC–FCT, followed by a FCT–BCT transformation at a lower temperature. Both of the transformation temperatures decrease as the palladium concentration increases, but the slope of the FCC–FCT boundary is smaller than that of the FCT–BCT boundary.

2.5. X-ray measurement of lattice parameters

X-ray measurements were performed with a SCINTAG XDS 2000 Wide-Angle X-ray Scattering Diffractometer which uses a source with a wavelength of 1.540 Å. This instrument is equipped with a temperature stage with a range of −270 to 300°C and maximum temperature rate of 30 °C/min. During the X-ray analysis, samples were scanned from $2\theta = 8°$ to 100° at various temperatures. The 2θ range covers most of the diffraction peaks. The 2θ angle was increased by 0.05° per step with a dwell time of 0.5 s. The samples were held at each temperature for one minute before making the X-ray

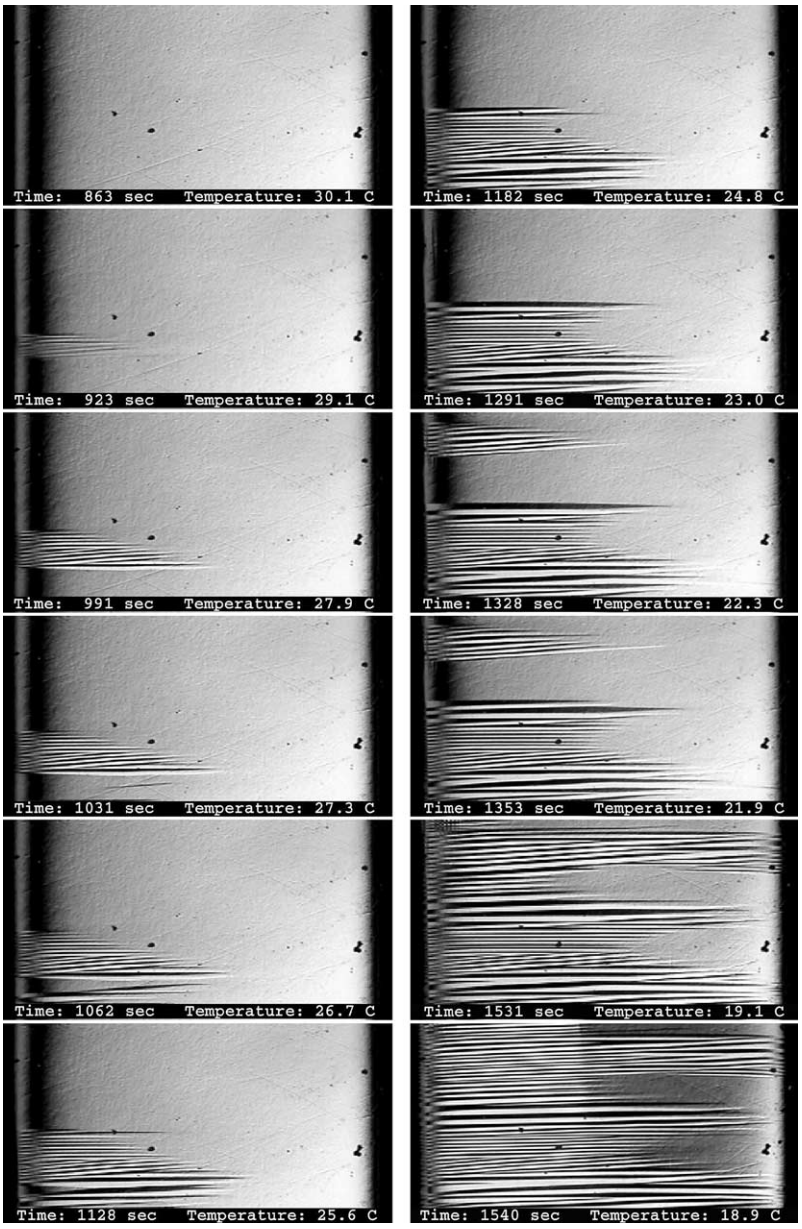

Fig. 4. Microstructures observed on the surface of specimen FePd4-MM6 during cooling are shown. The caption in each figure gives the test time in seconds and temperature in degree Celsius at which the image was taken. The specimen width is 2 mm and it is oriented with cubic [1 0 0] and [0 1 0] axes vertical and horizontal in these images.

measurement. The maximum rate of 30 °C/min was used to change the specimen temperature between measurements. The resulting diffraction patterns were analyzed and the information such as phase transformation temperatures and lattice parameters were obtained. Sample T3 was used for measurement of phase transformation temperatures and lattice parameters using this method. A 3D plot of the intensity of the diffracted X-ray beams versus temperature and 2θ angle is shown in Fig. 8. It clearly shows that the (2 2 0) FCC peak splits into two FCT peaks (2 2 0) and (2 0 2) with decreasing temperature. Lattice parameters were calculated from the values of 2θ at the peak intensities and they are summarized in Fig. 9. This figure indicates that the FCC–FCT transformation is a first-order transformation because of the coexistence of the austenite and the martensite phases, and the sudden jump of c/a ratio at about 38 °C. The average lattice parameters are $a = 3.822 \pm 0.001$ Å and $c = 3.630 \pm 0.001$ Å for the martensite, and $a_0 = 3.756 \pm 0.001$ Å for the austenite.

2.6. Latent heat measurements

Latent heat measurements were performed with a Perkin Elmer Thermal Analysis Differential Scanning Calorimeter (DSC) model Pyris^{TM} 1. Sample DSC-B2

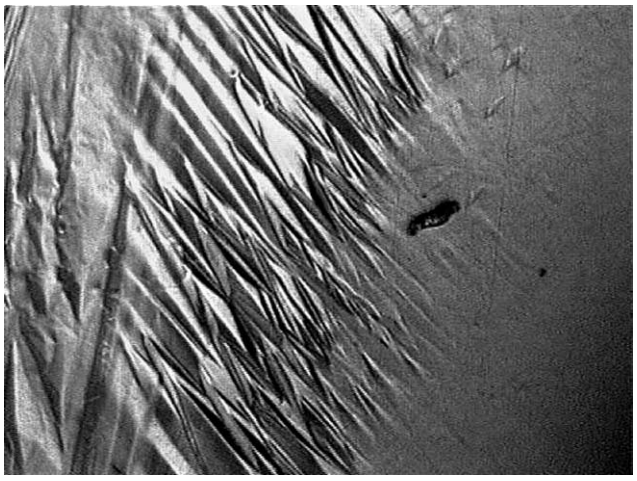

Fig. 5. An image of BCT microstructure in a matrix of FCT during the FCT–BCT phase transformation is shown. The temperature is −90 °C, the sample is FePd4B, which was heat treated. The field of view is 2 mm.

with a mass of 44.6 mg was used for these measurements. It was first polished at 60 °C to verify the existence of the FCC–FCT transformation. The results from sample DSC-B2 at a temperature rate of 10 °C/min are given in Fig. 10. Calculations using the areas under the peaks and above lines tangent to the linear parts of the curves give latent heats of 1.244 J/g (10.698 J/cm^3) for cooling and 1.267 J/g (10.896 J/cm^3) for heating. The magnitude of the latent heat in Fe_7Pd_3 is almost six times smaller than that of Ni_2MnGa (60.15 J/cm^3) (unpublished), and approximately five times smaller than that of CuAlNi (∼50 J/cm^3) [30]. In addition, the curves have multiple peaks indicating that the transformation is not continuous. The measurement was also repeated at a scanning rate of 1 °C/min, but the curves do not show any significant peaks except one at about 21 °C during the heating run. This is due to the small latent heat of the material, at this rate the heat flux is below the sensitivity of the instrument. This is also why a rather large sample was used. The measurements at 10 °C/min were found to be repeatable.

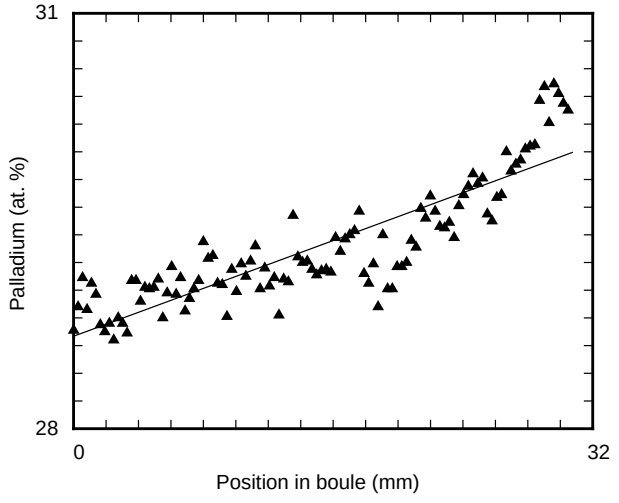

Fig. 6. Composition variation in single crystal boule FePd4 along its long axis is shown.

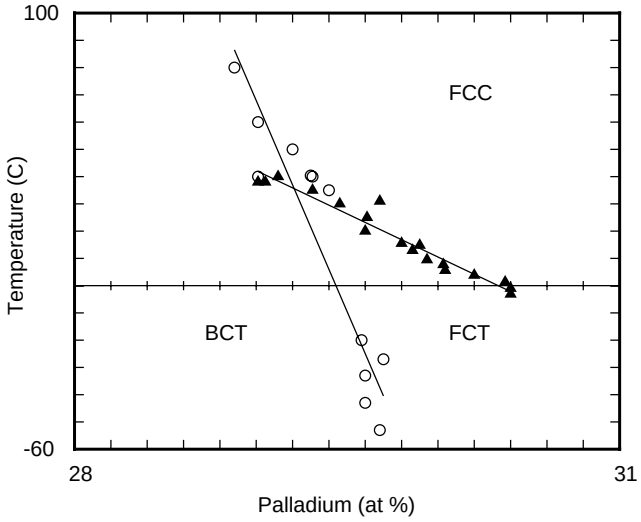

Fig. 7. Phase transformation temperatures for the FCC–FCT and FCC/FCT–BCT transformations versus palladium concentration are shown. All temperatures are for the start of transformation on cooling.

3. Magnetic properties

In this section various magnetic properties of both the austenite and martensite phases are reported. These include the Curie temperature of the austenite and the M–H curves for both phases in several crystallographic directions. The latter measurements allow the magnetic anisotropy constants to be calculated.

3.1. Susceptibility measurements procedure and curie temperature

The Curie temperature measurements were performed with a KLY-2 AC Susceptibility Kappa bridge. A polycrystalline specimen labeled FePd-exp222 was prepared using an arc melting furnace, and subjected it to homogenization at 1100 °C for 72 h in a quartz tube under vacuum. The specimen was then re-heated to 900 °C and held there for 120 min before being quenched in ice water.

The result of the susceptibility measurement is given in Fig. 11. It shows that the Curie temperature is about 450 °C, which is close to the results of Hansen [31], who reported 490 °C. The Curie temperature measurements were repeated few times and the results are consistent. The large change in susceptibility at 300 °C makes this temperature the effective limit of the usefulness of this alloy, even though it is ferromagnetic up to 450 °C.

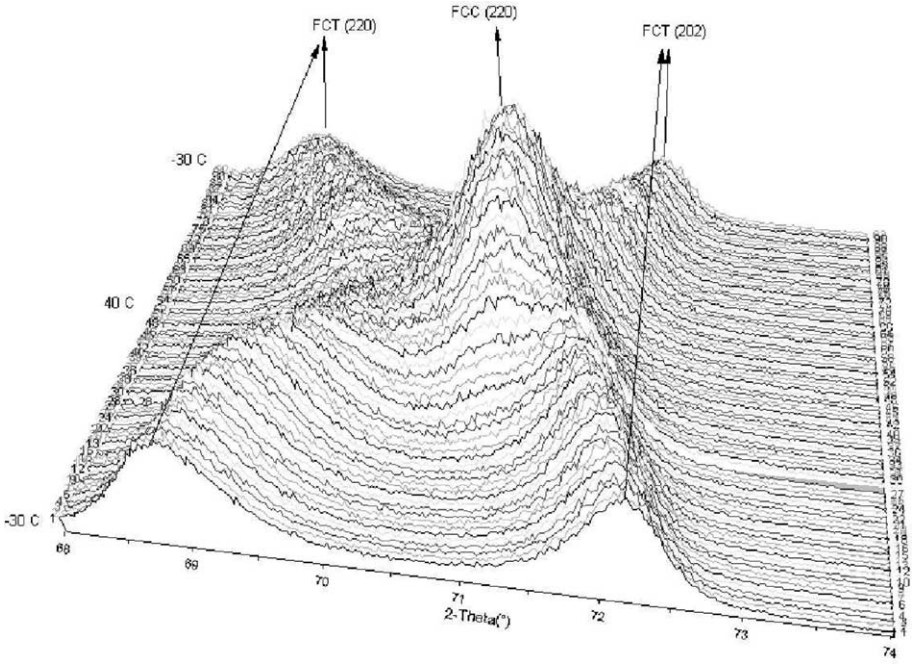

Fig. 8. The X-ray diffraction results versus temperature from −30 to 40 °C and from 40 to −30 °C for specimen T3 are shown. The temperature was increased from −30 °C (front of the plot) raised to 40 °C (middle of the plot) and lowered back to −30 °C (back of the plot). The two FCT peaks shift toward each other as temperature increases and eventually become one FCC peak.

3.2. Sample preparation and experimental procedure for magnetic anisotropy measurements

The austenite magnetic measurements were performed on specimen T5, a thin circular disk 9 mm in diameter and 0.36 mm thick. It was oriented with a $(1\bar{1}0)$ normal to give [0 0 1], [1 1 0], and [1 1 1] directions in plane of the disk as shown in Fig. 12. The disk was cut on an EDM (Electrical Discharge Machine) at 60 °C which kept the specimen at austenite state. After cutting, the specimen was retested with the X-ray microdiffractometer at 60 °C to verify the proper orientation. Specimen T5 is a disk, so that M–H curves in any in-plane direction may be directly compared. The EDM cutting and orientation verification procedure were also applied to specimens T3 and T6, which are used for the martensite measurements. Specimens T3 and T6 are thin rectangular plates with dimensions of $5.24 \times 4.89 \times 0.51$ mm^3. They are rectangular so that a compressive stress may be applied to the 4.89 mm faces. Specimen T3 has a

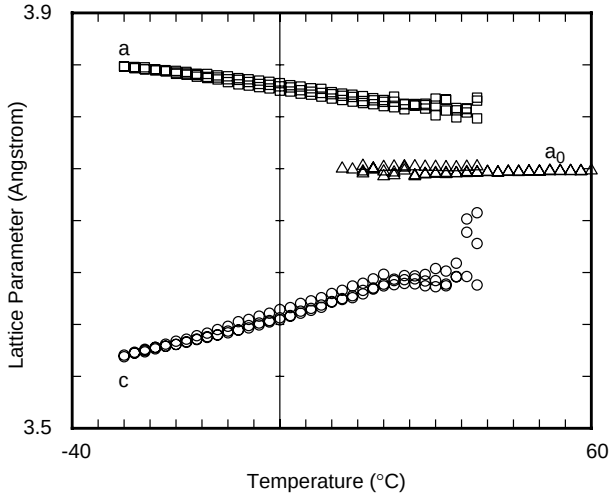

Fig. 9. The lattice parameters, a_0 of the cubic austenite and a and c of the tetragonal martensite, versus temperature for Fe_7Pd_3 specimen T3.

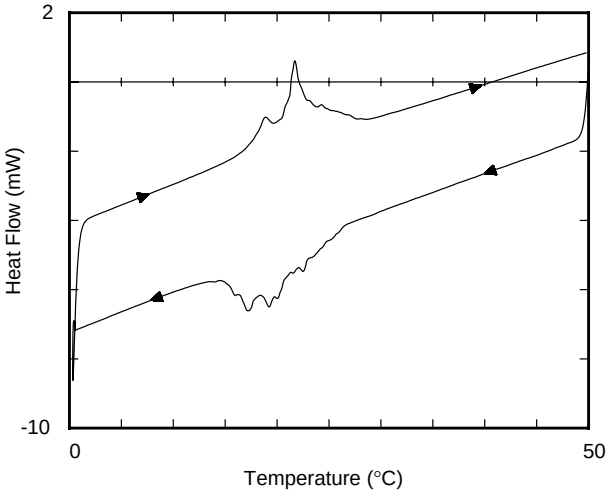

Fig. 10. The DSC curves for sample DSC-B2 at a heating/cooling rate of 10 °C/min. The bases of the DSC curves are connected to calculate the areas under the peaks, which are the latent heats. The latent heats are 1.267 J/g on heating and 1.244 J/g on cooling.

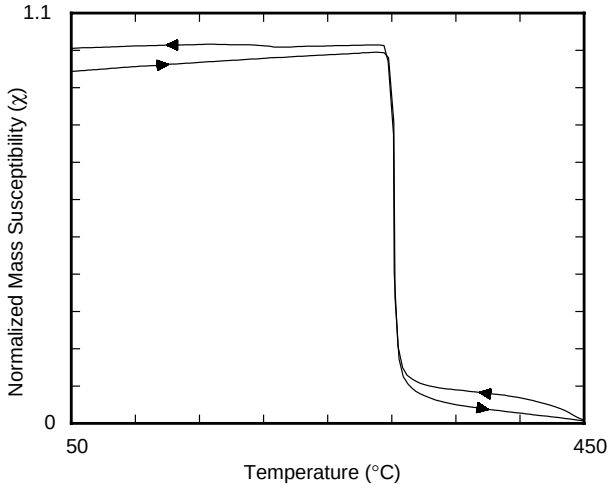

Fig. 11. Normalized mass susceptibility of Fe_7Pd_3 as a function of temperature is shown. The Curie temperature is 450 °C.

[1 $\bar{1}$ 0] surface normal with a [0 0 1] edge, while specimen T6 was oriented with a [0 $\bar{1}$ 0] surface normal and a [0 0 1] edge, see Fig. 12. In addition, samples T3, T5, and T6 were heat treated at 900 °C for 120 min and quenched in NaOH 10 wt.% solution at −8 °C.

The geometry of the specimens was chosen to give desired demagnetization factors. Specimen T5 is a disk, so that all magnetization directions in the plane of the specimen have equal demagnetization factors and thus can be directly compared. Specimens T3 and T6 in the austenite (as machined) state are rectangular so that the specimen is approximately square (they were cut using preliminary lattice parameters and so will not be exactly square) when compressed from austenite to a single variant state. A square shape results in equal demagnetization factors in the plane of these specimens in the single variant state. The demagnetization factor in the direction of the easy axis of the material also affects the M–H curves. Because this is a magnetically soft material, the demagnetized state of the material will be one that minimizes the sum of the anisotropy and stray field energies. The easy axis direction minimizes the anisotropy energy and if this is also a direction of minimum demagnetization factor, then this also minimizes the stray field energy. However, if the easy axes are not directions with small demagnetization factors, the demagnetized state can be assumed to contain more material that is not magnetized in the easy direction. The M–H curves are affected by the initial demagnetized state. If the initial state contains less material magnetized in the easy direction, then applying a field in a hard direction (a direction with a lower demagnetization factor than the easy direction) will result in an easier M–H curve. This will be seen to be the case in specimen T3 which has easy [1 0 0] directions that do not lie in the plane of this thin plate specimen. Magnetization of specimen T3 in the [0 0 1] direction will be easier than magnetizing specimen T6 (which has [1 0 0] directions in its thin plane) in the same direction because of the effect of demagnetization on the initial demagnetized state.

Magnetization measurements were performed in three crystallographic directions on the austenite and martensite. Magnetization measurements were made on the austenite (specimen T5) at 60 °C in the [1 0 0], [0 1 1] and [1 1 1] directions. The martensite (specimens T3 and T6) was measured in the directions [1 0 0] (*a*-axis), [0 1 1] and [0 0 1] (*c*-axis) at −20 °C. During the measurements of martensite magnetization, a constant compression was applied to the specimen to ensure the single variant state. The compression fixture was constructed from a non-magnetic CuBe spring alloy and was sized to fit in the temperature chamber used with the VSM [5], see Fig. 13. A small set screw on the fixture allowed a fixed amount of extension to be set which applied a corresponding compressive stress to the specimen. The stress was calculated from the total displacement of the fixture minus the contraction of the specimen due to the phase transformation multiplied by the spring constant of the fixture, which was characterized by a tensile test. Because of the unknown thermal strains in Fe_7Pd_3 and the phase transformation, it was not possible to correct the applied stress for thermal strains and it is expected that there are some variations from the nominal stress values reported here, which are at room temperature.

Materials that are magnetically anisotropic store different amounts of energy depending on the direction of the magnetization. For materials with cubic symme-

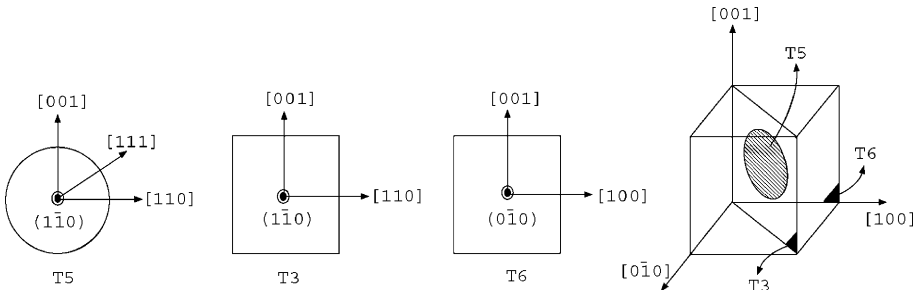

Fig. 12. Schematic drawings of samples T3, T5, and T6 and their orientations are shown.

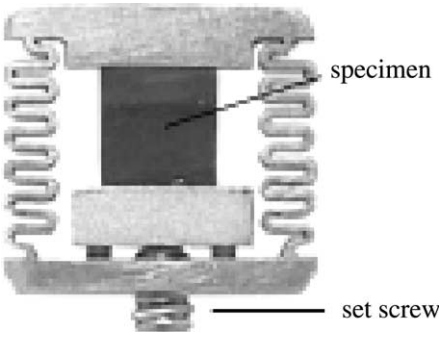

Fig. 13. A picture of the fixture used to apply compressive stress to specimens T3 and T6 in the [0 0 1] direction is shown. This fixture was originally constructed for the work reported in [5].

try this energy, E_C, is written in terms of the direction cosines of the magnetization, α_i, to the cubic axes and the anisotropy constants, K_i. Bozorth [32] gives the first three terms of E_C as

$$E_C = K_0 + K_1(\alpha_1^2\alpha_2^2 + \alpha_1^2\alpha_3^2 + \alpha_2^2\alpha_3^2) + K_2\alpha_1^2\alpha_2^2\alpha_3^2. \quad (1)$$

The area under an M–H curve is

$$W_{hkl} = \int_0^{M_s} H\,\mathrm{d}M, \quad (2)$$

where M_s is the magnetization saturation value of the material and *hkl* are the indices of the crystallographic direction of the applied field. The difference in W_{hkl} for two directions is equal to the difference in E_C for these directions [32] and this can be used to determine the anisotropy constants from the M–H curves in several directions as

$$\begin{aligned} K_0 &= W_{100}, \\ K_1 &= 4(W_{110} - W_{100}), \\ K_2 &= 27(W_{111} - W_{100}) - 36(W_{110} - W_{100}). \end{aligned} \quad (3)$$

Tetragonal materials may be treated in a similar manner and in this case Bozorth [32] gives the energy as

$$E_T = K_0 + K_1\sin^2\phi + K_2\sin^4\phi + K_3\cos^2\alpha\cos^2\beta, \quad (4)$$

where ϕ is the angle between the magnetization and the *c*-axis ([0 0 1]) and α and β are the angles between the magnetization and the *a*-axes ([1 0 0] and [0 1 0]). These four constants can be related to differences between areas under magnetization curves in different directions as above to give

$$\begin{aligned} K_0 &= W_{001}, \\ K_1 + K_2 &= W_{100} - W_{001}, \\ K_3/4 &= W_{110} - W_{100}. \end{aligned} \quad (5)$$

It is not possible to determine K_1 and K_2 separately from directional information alone, instead a fit to the shape of the M–H curve is required and will not be considered here.

The magnetization curves were measured with a Princeton Applied Research VSM. Temperature control was achieved by using an acrylic specimen enclosure, which fit between the pole pieces of the VSM, through which cooled or heated nitrogen gas flowed. A small T-type non-magnetic thermocouple was in direct contact with the back the specimen. For the duration of measurement, the specimen temperature was controlled within 1–2 °C by adjusting the gas flow rate. After the anisotropy measurements, the specimens were checked by X-ray analysis to verify the existence of phase transformation, and the anisotropy measurements were repeated after the X-ray analysis. The M–H curves reported here have had the usual para-magnetization correction applied.

3.2.1. Measurements of the magnetic anisotropy of austenite

The M–H curves of the austenite at 60 °C are shown in Fig. 14. The curves for the different orientations are too close together to distinguish them in the figure. The austenite saturation magnetization, m_s, is 1080 ± 10 emu/cm^3 at 60 °C. Several of these measurements were performed on the same specimen at various temperatures and the results are summarized in Table 2. The negative value of K_1 indicates that the easy axis of the austenite is along the [1 1 1] direction, but the preference for [1 1 1] is slight.

3.2.2. Measurements of the magnetic anisotropy of martensite

Magnetization measurements on martensite were performed at temperatures of 20, 10, 0, and −20 °C and under stresses of 0, −2, and −8 MPa in the [0 0 1] direction. Typical M–H curves are shown in Fig. 15, which are for sample T6 at a temperature of −20 °C and under stresses of 0, −2, −8 MPa and in Fig. 16, which gives M–H curves for the [1 0 0], [1 1 0], and [0 0 1]

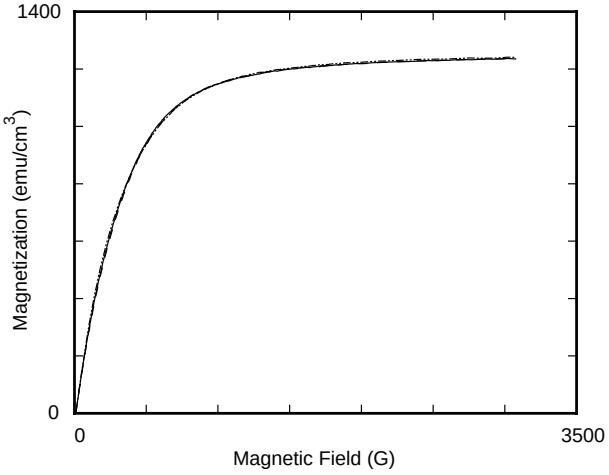

Fig. 14. The M–H curves for specimen T5 in the austenite state are shown for three directions of applied magnetic field. There are three curves present for the [1 0 0], [1 1 0], and [1 1 1] directions that are indistinguishable.

Table 2
Summary of Fe_7Pd_3 cubic magnetic anisotropy constants for the austenitic phase is given at three temperatures

Temperature (°C)	K_0 ($\times 10^5$ erg/cm^3)	K_1 ($\times 10^3$ erg/cm^3)	K_2 ($\times 10^4$ erg/cm^3)
60	3.48	−5	−6.6
50	3.58	−8	−3.5
40	3.66	−2	−18.4
30	3.77	−30	−9.4
22	3.94	−46	−4.7

The uncertainty in these results is $\pm 2 \times 10^3$ erg/cm^3.

directions at −20 °C and −8 MPa. Data were collected from all combinations of these temperatures and stresses and they are reported in Tables 3–5 as the tetragonal anisotropy constants given in Eq. (5). The martensite saturation magnetization is found to be 1220 ± 10 emu/cm^3 at −20 °C.

The anisotropy constant of primary interest is $K_1 + K_2$ given in Table 4. The data in this table show two major trends. The anisotropy of the martensite increases both with increasing compressive stress and with decreasing temperature. Both effects tend to increase the volume fraction of a single variant of the martensite. In a completely unbiased state, a microstructure with equal amounts of all three variants would appear isotropic. As discussed above, application of applied stress along the [0 0 1] direction of the crystal will favor the variant with its *c*-axis in this direction. Increasing compressive stress at −20 °C has the largest effect on the anisotropy as the transformation to martensite is most complete at this temperature. The data point at 0 °C and 0 MPa does not fit the trends of the other points and clear explanation for this behavior is known.

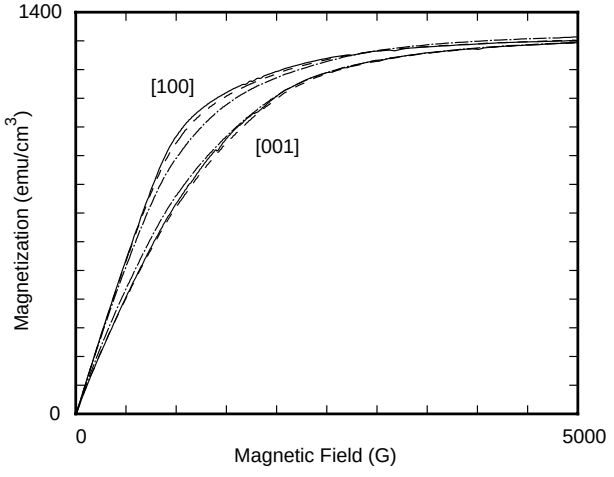

Fig. 15. Several M–H curves for specimen T6 with the applied field along the [1 0 0] and [0 0 1] directions are shown. The specimen temperature was held at −20 °C, and applied stresses of 0, −2, and −8 MPa were used. The upper curves are for the [1 0 0] axis and the lower set for the [0 0 1] axis. The solid curves are at an applied stress of −8 MPa, dashed at −2 MPa and dot-dashed at 0 MPa.

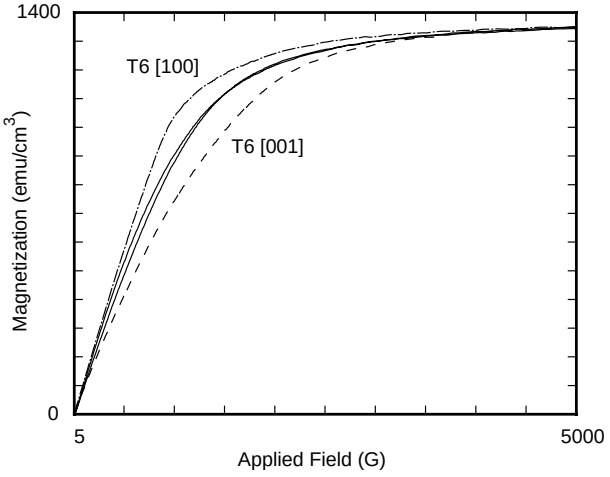

Fig. 16. The M–H curves of specimens T3 and T6 at −20 °C are shown for a compressive stress of −8 MPa on their [0 0 1] directions. The solid curves are from specimen T3, the orientation [0 0 1] curve is above the [1 1 0] curve. The specimen T6 curves are dashed for the [0 0 1] orientation and dot-dashed for the [1 0 0] orientation.

The data in Fig. 15 show that the [1 0 0] (*a*-axis) direction is easier that the [0 0 1] (*c*-axis) direction. This clearly establishes that the [0 0 1] direction is not the easy direction in this material. For tetragonal symmetry the remaining choices are an easy (0 0 1) plane or a pair of easy directions in the [1 0 0] and [0 1 0] directions. The data in Fig. 16 shows that the [1 0 0] direction is slightly easier than the [1 1 0] direction. This indicates that the martensite has a pair of easy axes, but the difference from an easy plane is small compared to the difference between the [1 0 0] and [0 0 1] directions.

To further support the conclusion that [0 0 1] is the hard axis, one more measurement was performed on specimen T3 with the applied magnetic field in the [0.087, 0.087, 0.992] direction, which is 5° from the [0 0 1] direction toward the [1 1 1] direction. This measurement was done at −20 °C and under −8 MPa of applied stress in the [0 0 1] direction. If the change in demagnetization factor is neglected for this small amount of rotation, this result can also be compared to the previous results. The M–H curve in the [0.087, 0.087, 0.992] direction was found to be easier than the curve for the [0 0 1] direction.

Comparison of all M–H curves, including ones not presented here, shows that they all possess three common

Table 3
Tetragonal anisotropy constant K_0 ($\times 10^6$ erg/cm^3) at various temperatures and stresses for Fe_7Pd_3 sample T6 is given

Stress (MPa)	Temperature (°C)			
	20	10	0	−20
0	0.910	1.073	1.224	1.362
−2	0.966	1.090	1.168	1.419
−8	1.008	1.103	1.211	1.398

The uncertainty in these results is $\pm 2 \times 10^3$ erg/cm^3.

Table 4
Tetragonal anisotropy constant $K_1 + K_2$ ($\times 10^5$ erg/cm^3) at various temperatures and stresses for Fe_7Pd_3 sample T6 is given

Stress (MPa)	Temperature (°C)			
	20	10	0	−20
0	−0.14	−1.22	−2.28	−1.93
−2	−0.51	−1.33	−1.68	−3.35
−8	−0.91	−1.47	−2.29	−3.44

The uncertainty in these results is $\pm 2 \times 10^3$ erg/cm^3.

Table 5
Tetragonal anisotropy constant $K_3/4$ ($\times 10^5$ erg/cm^5) at various temperatures and stresses for Fe_7Pd_3 sample T3 is given

Stress (MPa)	Temperature (°C)			
	20	10	0	−20
0	1.82	1.48	1.15	−0.07
−2	2.20	2.04	1.53	1.17
−8	2.13	1.86	1.73	1.21

The uncertainty in these results is $\pm 2 \times 10^3$ erg/cm^3.

features: first, all the [1 1 0] curves are close to each other regardless the changes of temperature and stress; second, similar to the [1 1 0] curves, all the [0 0 1] curves are very close together; third, all the [0 0 1] curves are magnetically easier than the [1 1 0] curves when the applied fields are less than about 1400–1600 G. This behavior is related to the details of the rotation of the magnetization under applied field towards the final saturated state from the demagnetized state as discussed above.

Conventionally magnetostrictive materials become anisotropic on the application of applied stress. However the the low stresses applied here would only account for about 1% of the anisotropy observed, assuming that the magnetostriction constant for Fe_7Pd_3 was in the typical range of $\lambda_s \approx 10^{-5}$. In these types of materials it is hard to separate conventional magnetostriction from variant rearrangement, but because of the martensitic behavior observed in this material, it is assumed that this measured anisotropy is an intrinsic martensite single variant property. In addition, stress induced anisotropy would not lead to the ferromagnetic shape-memory behavior observed in this material. It is not possible to directly compare the applied stress levels to the stress required to move twin boundaries because of specimen shape and microstructural interaction effects. These effects make it hard to isolate the stress needed to move twin boundaries and quantify the stress needed to move twins for a particular specimen and microstructure geometry.

4. Conclusions

The measurements of the thermomechanical properties of Fe_7Pd_3 presented above show that this alloy undergoes a first-order structural phase transformation. The latent heat and lattice parameter measurements confirm this. However, the latent heat is an order of magnitude smaller than other shape-memory materials and the lattice parameters continue to vary with temperature below the transformation temperature. Thus it appears to be a weakly first-order material, which agrees with Oshima [15] who reports it as ''close to second-order''. On the other hand, difference in the austenite and martensite lattice parameters is quite large so in that sense it is not near second-order.

Shape-memory materials such as CuAlNi and NiMnGa show a sharp interface between austenite and finely twined martensite. However, the microstructures in Fig. 4 do not have this structure. Instead the martensite appears in form of needles in an austenite matrix and many of the austenite–martensite interfaces are curved. Calculations using the crystallographic theory of martensite [33] show that one of the A–M interfaces in Fe_7Pd_3 should be close to 45° in Fig. 4. The tips of the martensite needles observed in Fe_7Pd_3 do tend to line up along 45° lines, sometimes in a very pronounced manner. This would roughly correspond to an austenite – very coarsely twinned martensite interface. This behavior and the presence of curved interfaces indicates that there is not a large amount of elastic energy associated with these microstructures. In theoretical terms this appears to indicate that the microstructures in this material cannot be predicted accurately by constrained theory [34], which ignores elastic strains.

The boules of Fe_7Pd_3 grown thus far have had significant composition changes along their length. One possible solution is to perform the growth process twice, inverting the boule between the two runs. For now, this variation has been used to assess the behavior of this alloy over a small range of compositions. The phase diagram developed in Fig. 7 shows that the transformations in this alloy are very sensitive to composition changes. This measurement is in good agreement with the results from Oshima [13–16] except the minor difference in the transition temperatures. For FSM behavior it is necessary to avoid transformations to the BCT structure while maintaining the highest possible FCC–FCT transformation temperature. A composition with 30 at.% appears to be a good choice based on Fig. 7.

All of the magnetic measurements presented here support the conclusion that Fe_7Pd_3 in the tetragonal martensitic phase has easy axes in the [1 0 0] and [0 1 0] (a-axes) directions while [0 0 1] (c-axis) is the hard direction. Magneto-mechanical measurements [35] also agree with these conclusions. An Fe_7Pd_3 specimen under uniaxial compression lengthens when a magnetic field is applied along the same direction as the compression. This choice of axes agrees with a previous study by James and Wuttig [7], but disagrees with [29] and DFT calculations [36]. The reasons for these discrepancies are not clear. The austenite was found to be only weakly anisotropic. The

saturation magnetization of the austenite was found to be 1080 emu/cm^3 at 60 °C which is slightly lower than the value of 1220 emu/cm^3 at −20 °C found for the martensite. The area between the [0 0 1] hard axis and [1 0 0] easy axis for the martensite was found to be about $3.44 \pm 0.02 \times 10^5$ erg/cm^3. This result is roughly one order of magnitude smaller than the polycrystal measurements in the literature [29]. The Curie temperature for this alloy was measured to be 450 °C which is well above the structural transformation temperatures for all the compositions considered here. Thus both the austenite and martensite phases near the structural transformation temperatures are ferromagnetic.

The anisotropy measurements at various temperatures and stresses for samples T6 and T3 are summarized in Fig. 16 and Tables 3–5. For sample T6, these tables show that both temperature and stress have an effect on the magnetic anisotropy. However, these are primarily due to the extent that martensite is detwinned by biasing stress. At a temperature of −20 °C an increase in stress from −2 to −8 MPa results in an increased anisotropy $(K_1 + K_2)$ of 0.09×10^5 erg/cm^3, while an increase in the stress from 0 to −2 MPa results in an increased anisotropy of 1.42×10^5 erg/cm^3. This indicates that the sample is approaching its fully detwinned state under −8 MPa of compression. Thus a temperature of −20 °C and a stress of −8 MPa should be used as the minimum conditions for measuring the magnetic anisotropy of a single variant of martensite, however, the temperature cannot be lowered significantly nor the amount of compression significantly increased without causing the undesirable FCT–BCT transformation. Because [1 1 0] M–H curve is in between the M–H curves for the hard and easy directions, the material does not have an easy plane.

Acknowledgements

We would like to thank the Department of Defense through the Office of Navy Research [Grant Nos. N00014-91-J-4034, N00014-01-1-0761 (MURI program), and N00014-99-1-0635 (DURIP program)] and the National Science Foundation (Grant No. NSF-0074043) for supporting this research.

References

[1] Shield TW. Orientation dependence of the pseudoelastic behavior of single crystals of Cu–Al–Ni in tension. J Mech Phys Solids 1995;43:869.
[2] Shimizu K, Kakashita T. Effect of magnetic fields on martensitic transformations in ferrous alloys and steels. ISIJ Int 1989;29:97.
[3] Malinen PA, Sadovskii VD, Smirnov LV, Fokina YA. Reasons for the influence of a pulsating magnetic field on martensitic transformation in steels and alloys. Fiz Metal Metalloved 1967;23(3):535.
[4] Clark A. Ferromagnetic materials. Amsterdam: North-Holland; 1980.
[5] Tickle R, James RD. Magnetic and magnetomechanical properties of Ni_2MnGa. J Magn Magn Mater 1999;195:627.
[6] Sozinov A, Likhachev AA, Ullakko K. Crystal structures and magnetic anisotropy properties of Ni–Mn–Ga martensitic phases with giant magnetic-field induced strain. IEEE Trans Magn 2002;38(5):2814.
[7] James RD, Wuttig M. Magnetostriction of martensite. Philos Mag A 1998;77(5):1273.
[8] Vasil'ev AN, Klestov SA, Levitin RZ, Snegirev VV. Magnetoelastic interaction in the martensitic transformation in an Ni_2MnGa single crystal. JETP 1996;82(3):524.
[9] Ullakko K, Huang JK, Kantner C, O'Handley RC, Kokorin VV. Large magnetic field induced strains in Ni_2MnGa single crystals. Appl Phys Lett 1996;69(13):1966.
[10] Tickle R, James RD, Shield T, Wuttig M, Kokorin VV. Ferromagnetic shape memory in the NiMnGa system. IEEE Trans Magn 1999;35(5):4301.
[11] O'Handley RC. Model for strain and magnetization in magnetic shape memory alloys. J Appl Phys 1998;83(6):3263.
[12] Tickle R. Ferromagnetic shape memory materials. Ph.D. thesis, University of Minnesota, 2000.
[13] Somura T, Oshima R, Fujita FE. Thermoelastic fcc–fct martensitic transformation in iron–palladium alloy. Scr Metall 1980;14(8):855.
[14] Oshima R. Successive martensitic transformations in iron–palladium alloys. Scr Metall 1981;15(8):829.
[15] Oshima R, Sugiyama M. Martensite transformations in iron–palladium alloys. J Phys, Colloq 1982;C(4):383.
[16] Sugiyama M, Oshima R, Fujita FE. Martensitic transformation in the iron–palladium alloy system. Trans Jpn Inst Met 1984;25(9):585.
[17] Sugiyama M, Harada S, Oshima R. Change in young's modulus of thermoelastic martensite iron–palladium alloys. Scr Metall 1985;19(3):315.
[18] Sugiyama M, Oshima R, Fujita FE. Mechanism of fcc–fct thermoelastic martensite transformation in iron–palladium alloys. Trans Jpn Inst Met 1986;27(10):719.
[19] Muto S, Oshima R, Fujita FE. Relation of magnetic domain structures to fct martensite variants in Fe–Pd alloys. Scr Metall 1987;21:465.
[20] Oshima R, Sugiyama M, Fujita FE. Tweed structures associated with fcc–fct transformations in iron–palladium alloys. Metall Trans A 1988;19A(4):803.
[21] Muto S, Takeda S, Oshima R, Fujita FE. High resolution electron microscopy of the tweed microstructure in an iron–palladium alloy. J Appl Phys Part 2 1988;27(8):1387.
[22] Oshima R, Tanaka K, Taniyama A, Fujita FE. Study of bct martensite of iron–palladium alloys. Mater Sci Forum 1990;56–58:175 (Martensitic Transform., Pt. 1).
[23] Muto S, Takeda S, Oshima R, Fujita FE. High resolution electron microscopy of tweed microstructure in iron–palladium alloys. Mater Sci Forum 1990;56–58:45 (Martensitic Transform., Pt. 1).
[24] Muto S, Oshima R, Fujita FE. Consideration of the tweed structure of iron–palladium alloys by continuum elasticity theory. Mater Sci Forum 1990;56–58:65 (Martensitic Transform., Pt. 1).
[25] Muto S, Takeda S, Oshima R. Analysis of lattice modulations in the tweed structure of an iron–palladium alloy by image processing of a high resolution electron micrograph. J Appl Phys Part 1 1990;29(10):2066.
[26] Tanaka K, Oshima R. Role of annealing twin in the formation of variant structure of bct martensite in iron–palladium alloy. Mater Trans JIM 1991;32(4):325.
[27] Oshima R, Muto S, Fujita FE. Initiation of fcc–fct thermoelastic martensite transformation from premartensitic state of iron-30 at.% palladium alloys. Mater Trans JIM 1992;33(3):197.

[28] Tanaka K, Hiraga K, Oshima R. Origin of tetragonality of bct martensite in substitutional iron–palladium (-nickel) disordered alloys. Mater Trans JIM 1992;33(3):215.
[29] rMatsuui M, Kuang JP, Totani T, Adachi K. Magnetic anisotropy of fepd invar alloys. J Magn Magn Mater 1986; 54–57(3):911.
[30] Cui J, James RD. A "Tent" shape thermoelastic deformation on foil of CuAlNi single crystal. AEM Report 2002-2, University of Minnesota Department of Aerospace Engineering and Mechanics, 2002.
[31] Hansen M. Constitution of binary alloys. 2nd ed. New York: McGraw-Hill; 1958.
[32] Bozorth RM. Ferromagnetism. IEEE Press; 1978.
[33] Ball JM, James RD. Fine phase mixtures as minimizers of energy. Arch Rational Mech Anal 1987;100:13.
[34] Ball JM, Chu C, James RD. Metastability of martensite, 1994 [preprint].
[35] Cui J, Shield TW, James RD. Ferromagnetic shape memory effects in an iron–palladium alloy, 2003 [preprint].
[36] Stern RA. Private Communication. Tulane University.